Original Article

MOLECULAR METABOLISM

Sirt6 in pro-opiomelanocortin neurons controls energy metabolism by modulating leptin signaling

Qin Tang [1,2,6], Yong Gao [4,6], Qinhui Liu [2], Xuping Yang [1,2], Tong Wu [1,2], Cuiyuan Huang [1,2], Ya Huang [1,2], Jinhang Zhang [1,2], Zijing Zhang [1,2], Rui Li [1,2], Shiyun Pu [1,2], Guorong Zhang [1,2], Yingnan Zhao [1,2], Jian Zhou [1,2], Hui Huang [1,2], Yanping Li [1,2], Wei Jiang [3], Yongsheng Chang [5,**], Jinhan He [1,2,*]

ABSTRACT

Objective: Sirt6 is an essential regulator of energy metabolism in multiple peripheral tissues. However, the direct role of Sirt6 in the hypothalamus, specifically pro-opiomelanocortin (POMC) neurons, controlling energy balance has not been established. Here, we aimed to determine the role of Sirt6 in hypothalamic POMC neurons in the regulation of energy balance and the underlying mechanisms.

Methods: For overexpression studies, the hypothalamic arcuate nucleus (ARC) of diet-induced obese mice was targeted bilaterally and adenovirus was delivered by using stereotaxic apparatus. For knockout studies, the POMC neuron-specific Sirt6 knockout mice (PKO mice) were generated. Mice were fed with chow diet or high-fat diet, and body weight and food intake were monitored. Whole-body energy expenditure was determined by metabolic cages. Parameters of body composition and glucose/lipid metabolism were evaluated.

Results: Sirt6 overexpression in the ARC ameliorated diet-induced obesity. Conversely, selective Sirt6 ablation in POMC neurons predisposed mice to obesity and metabolic disturbances. PKO mice showed an increased fat mass and food intake, while the energy expenditure was decreased. Mechanistically, Sirt6 could modulate leptin signaling in hypothalamic POMC neurons, with Sirt6 deficiency impairing leptin-induced phosphorylation of signal transducer and activator of transcription 3. The effects of leptin on reducing food intake and body weight and leptin-stimulated lipolysis were also impaired. Moreover, Sirt6 inhibition diminished the leptin-induced depolarization of POMC neurons.

Conclusions: Our results reveal a key role of Sirt6 in POMC neurons against energy imbalance, suggesting that Sirt6 is an important molecular regulator for POMC neurons to promote negative energy balance.

Keywords Sirt6; POMC neurons; Leptin sensitivity; Obesity; Energy balance; Sympathetic nervous system

1. INTRODUCTION

Energy balance is maintained by the equilibrium of energy intake and energy expenditure [1,2]. Lasting positive energy balance caused by long-term increased food intake and/or decreased energy expenditure results in the storage of energy primarily as fat in adipose depots, which leads to body weight gain and obesity [1,2]. The molecular mechanisms that coordinate energy homeostasis are partially known. A well-established view is that both the central and peripheral mechanisms are involved in maintaining energy balance [3]. In the central nervous system (CNS), specialized neurons sense and integrate peripheral hormones (e.g., leptin and insulin) and nutrients (e.g., free fatty acids and glucose) to modulate various aspects of metabolism for maintaining normal food intake and energy metabolism [4,5].

Accumulating evidence indicates that, within the CNS, the hypothalamus is a hub for the homeostatic regulation of the whole-body energy homeostasis [4,6]. In particular, the arcuate nucleus (ARC) of the hypothalamus is critical for regulating energy intake and expenditure. There are two main, distinct, functionally antagonistic series of neurons within the ARC: the orexigenic neurons expressing neuropeptide Y and agouti-related peptide, and the anorexigenic neurons expressing pro-opiomelanocortin and cocaine- and amphetamine-regulated transcript (POMC neurons) [7,8]. POMC neuronal activation is catabolic, which is essential in the maintenance of negative energy

[1]Department of Pharmacy, State Key Laboratory of Biotherapy, West China Hospital of Sichuan University, Chengdu, Sichuan 610041, China [2]Laboratory of Clinical Pharmacy and Adverse Drug Reaction, State Key Laboratory of Biotherapy, West China Hospital of Sichuan University, Chengdu, Sichuan 610041, China [3]Molecular Medicine Research Center, West China Hospital of Sichuan University, Chengdu, Sichuan 610041, China [4]Science and Technology Innovation Center, Guangzhou University of Chinese Medicine, Guangzhou, Guangdong 510405, China [5]Tianjin Key Laboratory of Cellular and Molecular Immunology, Key Laboratory of Immune Microenvironment and Disease (Ministry of Education), Department of Physiology and Pathophysiology, Tianjin Medical University, Tianjin 300070, China

[6] Qin Tang and Yong Gao contributed equally to this work.

*Corresponding author. Department of Pharmacy, State Key Laboratory of Biotherapy and Cancer Center, West China Hospital of Sichuan University and Collaborative Innovation Center of Biotherapy, Chengdu, Sichuan, China. E-mail: jinhanhe@scu.edu.cn (J. He).

**Corresponding author. Department of Physiology and Pathophysiology, Tianjin Medical University, Tianjin 300070, China. E-mail: changy007@163.com (Y. Chang).

Received February 13, 2020 • Revision received March 28, 2020 • Accepted April 3, 2020 • Available online 9 April 2020

https://doi.org/10.1016/j.molmet.2020.100994

Abbreviations

ARC	arcuate nucleus
AUC	area under the curve
BAT	brown adipose tissue
CD	chow diet
CNS	central nervous system
eWAT	epididymal white adipose tissue
GTT	glucose tolerance test
HFD	high-fat diet
iWAT	inguinal adipose tissue
ITT	insulin tolerance test
NE	norepinephrine
POMC	pro-opiomelanocortin
PVN	paraventricular hypothalamic nucleus
SKM	skeletal muscle
TC	total cholesterol
TG	triglyceride
VMH	ventromedial hypothalamic nucleus
WAT	white adipose tissue
WT	wild-type

balance. Mutation in the *Pomc* gene, which encodes POMC, results in hyperphagia and obesity in both humans and rodents [9,10]. As the first-order neurons in the ARC, POMC neurons project axonal processes mainly to second-order neurons located in hypothalamic areas, such as the paraventricular hypothalamic nucleus (PVN), ventromedial hypothalamic nucleus (VMH), dorsomedial hypothalamus (DMH), and lateral hypothalamus (LH) [11], and in extrahypothalamic areas such as the brain stem and spinal cord. These second-order neurons integrate and further process the received information and project to multiple neurocircuits, leading to an integrated response on energy intake and expenditure. Elucidating the molecular mechanisms involved in POMC neurons exerting negative energy balance is of significance for combating obesity.

Sirt6 is a member of the mammalian sirtuin family (Sirt1-7), a kind of nicotinamide adenine dinucleotide- (NAD^+-) dependent deacetylase [12]. Studies have revealed its functions in multiple peripheral tissues in the regulation of various metabolic processes [13–15]. Sirt6-specific deficiency in the liver resulted in increased glycolysis, triglyceride synthesis, and fatty liver formation [13]. In pancreatic β cells, Sirt6 is important for glucose-stimulated insulin secretion, and activation of Sirt6 may help to improve insulin secretion [14]. In skeletal muscle, Sirt6 deletion impaired glucose and insulin homeostasis, reduced whole-body energy expenditure, and weakened exercise performance [15]. In addition, we previously reported that, in adipose tissues, Sirt6 significantly increased the transcriptional activity of adipose triglyceride lipase by decreasing the phosphorylation and acetylation of forkhead box protein O1, thus promoting the lipolytic activity of adipose tissues [16]. Moreover, Sirt6 is essential for the thermogenesis of brown and beige fat, and Sirt6 deficiency in adipose tissues predisposes mice to obesity and related metabolic syndrome [16,17]. Furthermore, we also revealed that the effect of Sirt6 on lipid mobilization promoted ketogenesis in the liver [18]. Thus, Sirt6 acts as a metabolic sensor and plays a crucial role in energy and lipid/glucose metabolism in peripheral tissues.

In addition to its well-characterized role in multiple peripheral tissues, evidence indicates that Sirt6, which is highly expressed in the CNS [19,20], also acts as a central regulator of somatic growth and obesity [21]. However, to date, the direct role of Sirt6 in POMC neurons controlling energy balance has not been established. We hypothesized that Sirt6 in POMC neurons within the ARC is a key molecular component of pathways protecting against excessive body weight gain and obesity. To test this, we investigated the metabolic consequences of gain or loss of Sirt6 in the mouse hypothalamus. We found the overexpression of Sirt6 in the ARC protected against diet-induced obesity, while Sirt6 deficiency in POMC neurons predisposed mice to obesity and metabolic syndrome under both a chow diet (CD) and high-fat diet (HFD). This obese phenotype observed in POMC neuronal Sirt6-deficient mice is at least partly due to the impaired leptin functions in POMC neurons, which results in increased food intake and reduced energy expenditure. These results suggest that Sirt6 is an important molecular regulator for POMC neurons to promote negative energy balance.

2. MATERIALS AND METHODS

2.1. Mice

Male mice in a C57BL/6J background were used for all experiments described in this study. *Sirt6*$^{loxP/loxP}$ mice and *Pomc*-Cre mice were purchased from the Jackson Laboratory (Bar Harbor, ME, USA). To generate mice lacking Sirt6 specifically in POMC neurons (hereafter PKO mice), *Sirt6*$^{loxP/loxP}$ mice were interbred with *Pomc*-Cre mice. The *Sirt6*$^{loxP/loxP}$ littermates (hereafter LoxP mice) were used as controls. Mice were allowed free access to water and a CD or HFD (Research diet, D12492, USA) for 12–16 weeks, and food was only withdrawn if the animal was required for an experiment. Tissue PCR genotyping analysis for determining the presence of the Cre-deleted *Sirt6* allele was performed as described [13]. All mice were bred and housed in a 12-hour light/dark cycle at a controlled temperature (22–24 °C) environment, unless indicated otherwise. All animal experiments were reviewed and approved by the Institutional Animal Care and Use Committee of Sichuan University.

2.2. Food intake studies

Mice were individually housed in cages to measure food intake. For daily food intake assay, food pellets were weighed at 8:00 a.m. each day for 5 continuous days, carefully accounting for spillage, and an average of 5-day food intake was calculated. For fasting-induced refeeding assays, the single-housed mice were deprived of food overnight, then a preweighed amount of food was placed in the cages, and the food intake was calculated for 1, 2, 4, 8, and 24 h.

2.3. Metabolic parameter measurements

Energy expenditure and locomotor activity were monitored by using metabolic chambers of a Comprehensive Laboratory Animal Monitoring System (CLAMS, Columbus Instruments, Columbus, OH, USA). Before data collection, all mice were acclimatized to the chambers for 48 h. Rectal temperature of mice was measured by a rectal probe attached to a digital thermometer (KEW, Nanjing, China).

2.4. Glucose tolerance tests (GTTs) and insulin tolerance tests (ITTs)

GTTs and ITTs were performed as we previously described [22]. For GTT, mice were fasted overnight. After determining basal blood glucose levels, mice fed with a CD or HFD were intraperitoneally administered 2 or 1.5 g/kg D-glucose, respectively. Blood glucose levels were measured from the tail vein by using a glucometer at 15, 30, 60, 90, and 120 min after administration. For ITT, mice were fasted for 4 h to empty the stomach. After measuring basal blood glucose

levels, mice received an intraperitoneal administration of insulin (0.5 U/kg with CD or 0.75 U/kg with HFD). Blood glucose levels were measured from tail blood as described above.

2.5. Biochemical analysis

Mice were killed with CO_2 after overnight fasting, and the whole blood was collected by cardiac puncture. The blood was centrifuged at 6,000 rpm for 10 min, and the supernatant serum was collected. Serum insulin, leptin, and adiponectin levels were measured by using a Rat/Mouse Insulin ELISA Kit (EZRMI-13K, Merck Millipore, Darmstadt, Germany), Mouse Leptin ELISA Kit (EZML-82K, Merck Millipore, Darmstadt, Germany), and Mouse Adiponectin RIA Kit (EZMADP-60K, Merck Millipore, Darmstadt, Germany), respectively.

Levels of hepatic triglycerides (TG) and total cholesterol (TC) were determined as described [18,23,24]. In brief, 150 mg liver tissue was homogenized with 1 mL phosphate-buffered saline (PBS). Total lipids were extracted with chloroform/methanol (2:1, v/v) and dissolved in 1% Triton-X 100 in ethanol. Hepatic TC and TG levels were measured by using commercial enzymatic assay kits, all performed according to the manufacturer's instructions.

2.6. Norepinephrine (NE) levels in inguinal adipose tissue (iWAT)

iWAT (500 mg) was homogenized in 1 mL buffer (4 mmol/L EDTA, 1 mmol/L $Na_2S_2O_5$, 0.01 N HCl, pH 7.0) and centrifuged for 13,000 rpm at 4 °C. The infranatant omitting the debris pellet and the top fat layer was used for NE measurement, determined by high-performance liquid chromatography (HPLC).

2.7. Cold-stress experiments

For cold exposure experiments, mice at 8 or 20 weeks of age were transferred from room temperature to 4 °C to be cold-challenged, with free access to food and water. Body temperature was monitored with a rectal probe connected to a digital thermometer.

2.8. ^{18}F-fluoro-2-deoxy-D-glucose (^{18}F-FDG) PET-CT imaging

To determine ^{18}F-FDG uptake in iWAT, LoxP and PKO mice fasting overnight and then intravenously injected with 750 μCi ^{18}F-FDG into the tail vein. At 30 min after the injection, mice underwent micro-PET/CT analysis, performed with an Inveon multimodal platform.

2.9. *Ex vivo* lipolysis of adipose tissue

The *ex vivo* lipolysis assay of adipose tissues was performed as described [25–28]. Briefly, 50 mg epididymal adipose tissue (eWAT) or iWAT was surgically removed and washed with PBS and then incubated for 1 h at 37 °C in phenol red-free DMEM. The medium was collected, and glycerol content was determined by a colorimetric assay.

2.10. Leptin function and sensitivity studies

Leptin sensitivity assays were performed as described [29–33]. Weight-matched mice (6 weeks old) with a CD were individually housed and intraperitoneally injected with vehicle (0.1% bovine serum albumin (BSA)) for 3 days before intraperitoneal injection of leptin (1 μg/g, Peprotech, Rehovot, Israel) twice daily at 7:00 a.m. and 7:00 p.m. for 3 consecutive days. Body weight and food intake were detected at baseline and on each day. Furthermore, other cohorts of PKO and LoxP mice (6 weeks old) were intraperitoneally administered 0.1% BSA or leptin (1 μg/g). At 45 min after injection, brains were collected and processed for phosphorylated signal transducer and activator of transcription 3 (p-STAT3) (Tyr705) immunohistochemistry or the hypothalamus was collected for p-STAT3 (Tyr705) immunoblotting.

Subcutaneous minipump implantation was performed as described [34]. Mice (6 weeks old) were administered leptin (delivery rate 500 ng/h) or saline by mini-osmotic pumps (model 1007D, Alzet, Cupertino, CA, USA) subcutaneously for 2 days. eWAT and iWAT were collected for further determination.

2.11. Electrophysiology

Whole-cell patch-clamp recordings of *Pomc*-tdTomato neurons from hypothalamic slices were conducted as previously reported [35]. Briefly, male mice (4–6 weeks old) were anesthetized and transcardially perfused with modified ice-cold artificial cerebrospinal fluid (ACSF), and an equimolar amount of sucrose was used to substitute for NaCl. The entire brain was removed and submerged in ice-cold, carbogen-saturated (95% O_2 and 5% CO_2) ACSF (126 mM NaCl, 2.8 mM KCl, 1.2 mM $MgCl_2$, 2.5 mM $CaCl_2$, 1.25 mM NaH_2PO_4, 26 mM $NaHCO_3$, and 5 mM glucose). Coronal sections (250 μm) were cut by using a Leica VT1000S Vibratome and then incubated in oxygenated ACSF at room temperature for at least 1 h before recording. Slices were removed to the recording chamber to equilibrate for 10–20 min and bathed in oxygenated ACSF (32–34 °C) at flow rate ~2 mL/min. The pipette solution for the whole-cell recording contained 120 mM K-gluconate, 10 mM KCl, 10 mM HEPES, 5 mM EGTA, 1 mM $CaCl_2$, 1 mM $MgCl_2$, and 2 mM MgATP, and 0.03 mM Alexa Fluor 594 or Alexa Fluor 350 hydrazide dye (pH 7.3) was included to identify the recorded neurons. Epifluorescence was used to target fluorescent cells when the light source was switched to infrared differential interference contrast imaging to obtain the whole-cell recording (Zeiss Axioskop FS2 Plus equipped with a fixed stage and a QuantEM:512SC electron-multiplying charge-coupled device camera). PC-connected pCLAMP programs and an Axopatch700B amplifier (Molecular Devices), low-pass filtered at 2–5 kHz, were used to record and analyze electrophysiological signals. Recording electrodes had resistances of 2.5–5 MΩ when filled with the K-gluconate internal solution. Input resistance was assessed by measuring voltage deflection at the end of the response to a hyperpolarizing rectangular current pulse step (500 ms of −10 to −50 pA). Slices were incubated with OSS_128,167 (100 μM, HY-107454, MCE, New Jersey, USA) for 8 h before recording to specifically inhibit Sirt6 [36,37]. Leptin (100 nM) was added to the ACSF for specific experiments. Solutions containing leptin were typically perfused for 2–4 min. Depolarization or hyperpolarization was determined only if the change in membrane potential was >2 mV in amplitude.

2.12. RNA extraction and quantitative RT-PCR assay

Methods used for RNA extraction and quantitative RT-PCR were described previously [23,38]. Briefly, total RNA from different tissues was extracted by using TRIzol Reagent (Invitrogen) and reverse-transcribed by using the iScript cDNA synthesis kit (Bio-Rad, Hercules, CA, USA). SYBR Green PCR Master Mix (Bio-Rad, Hercules, CA, USA) was used for detecting mRNA levels. Relative expression of genes was calculated by the comparative Ct method and normalized to that of 18 S ribosomal RNA. Primers are listed in Supplementary Table 1.

2.13. Western blot analysis

In brief, tissues were homogenized in lysis buffer, sonicated and cleared by centrifugation (12,000 g, 10 min). Protein concentration in the supernatant was determined by the BCA assay (Pierce; 23,227). Samples were separated by 10% SDS-PAGE, transferred to a nitrocellulose membrane, probed with antibodies overnight at 4 °C, and then incubated with corresponding secondary antibodies for 1 h at room temperature. Blots were visualized by using the LICOR Odyssey

System (Lincoln, NE, USA), and protein levels were normalized to the β-Tubulin level for each sample. Primary antibodies for western blot analysis are listed in Supplementary Table 2.

2.14. Histological analysis of liver and adipose tissues

Liver, eWAT, iWAT, and brown adipose tissue (BAT) were fixed in 10% neutral-buffered formalin for 48–72 h and then dehydrated and embedded in paraffin by a standard procedure and cut into 4 μm sections. For H&E staining, sections were stained with hematoxylin and eosin (H&E) according to the manufacturer's instructions. Primary and secondary antibodies for immunohistochemistry analysis are listed in Supplementary Table 2. The fat cell size of eWAT and iWAT was measured in H&E-stained sections of three individual samples in each group. The average diameter of adipocyte was analyzed by using NIH ImageJ. For Oil-red O staining of liver tissues, frozen sections (8 μm) were fixed in formalin and incubated with 0.5% Oil-red O solution.

2.15. Immunohistochemistry analysis of brain tissues

For immunostaining, coronal brain sections were incubated with primary antibodies overnight at 4 °C and then washed and incubated with respective secondary antibodies for 1 h at room temperature. Sections were stained with DAPI (50 mg/mL) for 2 min and then cover-slipped. Sections were photographed under a confocal laser scanning microscope, and colocalization was quantified visually in a blinded fashion. Primary and secondary antibodies for immunohistochemistry analysis are listed in Supplementary Table 2.

2.16. Stereotaxic virus injections into the hypothalamic ARC of mice

To explore the effect of Sirt6 overexpression in the hypothalamus, we used stereotaxic injections of adenovirus- (Ad-) GFP or Ad-Sirt6 into the hypothalamic ARC. Wild-type (WT) mice were fed with an HFD for 8 weeks to induce obesity before virus injections. The ARC was targeted bilaterally, and the virus was delivered at 0.1 μL/min for 5 min according to the following coordinates: −1.5 mm posterior to the bregma, ±0.3 mm lateral to the midline, and −5.85 mm below the surface of the skull by using stereotaxic apparatus and microinjection pump (RWD Life Science, Shenzhen, China). After surgery, mice were transferred to a heated blanket for recovery. Body weight and food intake were recorded daily for 6 consecutive days after the surgery. At the end of this experiment, tissues were dissected and collected for further analysis. The successful delivery of the virus in the ARC was verified in brain sections.

2.17. Statistical analysis

All data are presented as mean ± SEM. All statistical analyses were performed using GraphPad Prism, version 7.04 (San Diego, CA, USA). Statistical significance was determined by Student's *t*-test or ANOVA. $P < 0.05$ was considered statistically significant. The number of cohorts and the number of mice for each experiment are indicated in figure legends.

3. RESULTS

3.1. Sirt6 overexpression in the ARC ameliorates HFD-induced obesity

To determine the potential role of Sirt6 in the hypothalamus, we first assessed its expression under different nutritional states. Both the mRNA and protein expressions of Sirt6 were significantly reduced in the hypothalamus of fasting mice as compared with *ad libitum*-fed controls (Figure 1A, B), and in HFD- and *db/db*-induced obese models (Figure 1C–F). Next, we stereotactically injected Ad-GFP or Ad-Sirt6 into the ARC of HFD-induced obese mice (Figure 1G) and assessed its metabolic functions. Localization studies revealed successful delivery of the adenovirus in the ARC (Figure 1H), and Sirt6 overexpression was confirmed by western blot analysis (Supplementary Figure 1A). Sirt6 overexpression significantly decreased body weight (Figure 1I). The weight of eWAT and iWAT was also decreased (Figure 1J). H&E staining showed that Sirt6 overexpression decreased the size of adipocytes in both eWAT and iWAT (Supplementary Figure 1B, C). Consistently, the key components in lipolytic pathways such as phosphorylation of hormone-sensitive lipase (p-HSL) and perilipin-1 (p-Plin1) were significantly increased in eWAT and iWAT from mice injected with Ad-Sirt6 (Supplementary Figure 1D, E). Also, Ad-Sirt6-injected mice showed significantly lower daily food intake compared to controls (Figure 1K), and the expression of *Cox8b* in iWAT was upregulated (Figure 1L). These changes were associated with increased mRNA levels of hypothalamic *Pomc* (Figure 1M). Collectively, these results indicate that the hypothalamic Sirt6 plays a pivotal role in coordinating whole-body energy balance.

POMC neuron plays a key role in energy metabolism [9,10]. We then detected Sirt6 expression in hypothalamic POMC neurons by double-labeling immunofluorescence. The expression of Sirt6 was significantly decreased in POMC neurons of fasting, HFD-fed, and *db/db* mice as compared with their controls (Figure 1N,O). Consistently, FACS sorting of tdTomato-labeled POMC neurons in the hypothalamus further demonstrated reduced Sirt6 level in POMC neurons under an HFD compared with CD (Figure 1P). These results further support that Sirt6 in POMC neurons plays key roles in the central regulation of energy homeostasis.

3.2. Generation and validation of mice lacking Sirt6 in POMC neurons

To determine the specific role of Sirt6 in POMC neurons, we generated POMC neuron-specific Sirt6 knockout mice (PKO mice) by crossing *Sirt6*$^{loxP/loxP}$ mice (LoxP mice) with mice expressing Cre recombinase under the control of the *Pomc* promoter (Figure 2A). PCR genotyping analysis confirmed the specific expression of Cre recombinase in the hypothalamus (Supplementary Figure 2A). The expression of Sirt6 was consistently decreased in the ARC but not in other tissues from PKO mice (Figure 2B and Supplementary Figure 2B). Moreover, the deletion of Sirt6 in POMC neurons did not affect the mRNA levels of other sirtuin deacetylases in the ARC (Supplementary Figure 2C).

By crossing the *Pomc*-Cre or PKO mice with the mT/mG reporter mice, we generated two types of mouse models: *Pomc*-Cre/mT/mG mice and *Pomc*-Cre/*Sirt6*$^{loxP/loxP}$/mT/mG mice. Both strains carry the *Gfp* allele to allow for selective expression of GFP in POMC neurons. Because Sirt6 has been reported to exert neuroprotective actions [39], we assessed whether Sirt6 deletion affected the development or survival of POMC neurons in the hypothalamus. Anatomical evaluation of POMC neurons throughout the hypothalamus of LoxP and PKO mice revealed no alterations in neuronal distribution of somatic area (Supplementary Figure 2D–F). In the pituitary, no significant differences in Sirt6 expression, corticotroph cell number, or pituitary-related genes were observed between LoxP and PKO mice (Supplementary Figure 2B, G, H).

3.3. Deletion of Sirt6 in POMC neurons causes obesity

PKO mice at 6 weeks of age were morphologically normal and displayed comparable blood glucose levels under *ad libitum* and fasting conditions (Supplementary Figure 3A, B). Furthermore, the body length of PKO mice at 6 weeks of age was comparable with LoxP controls

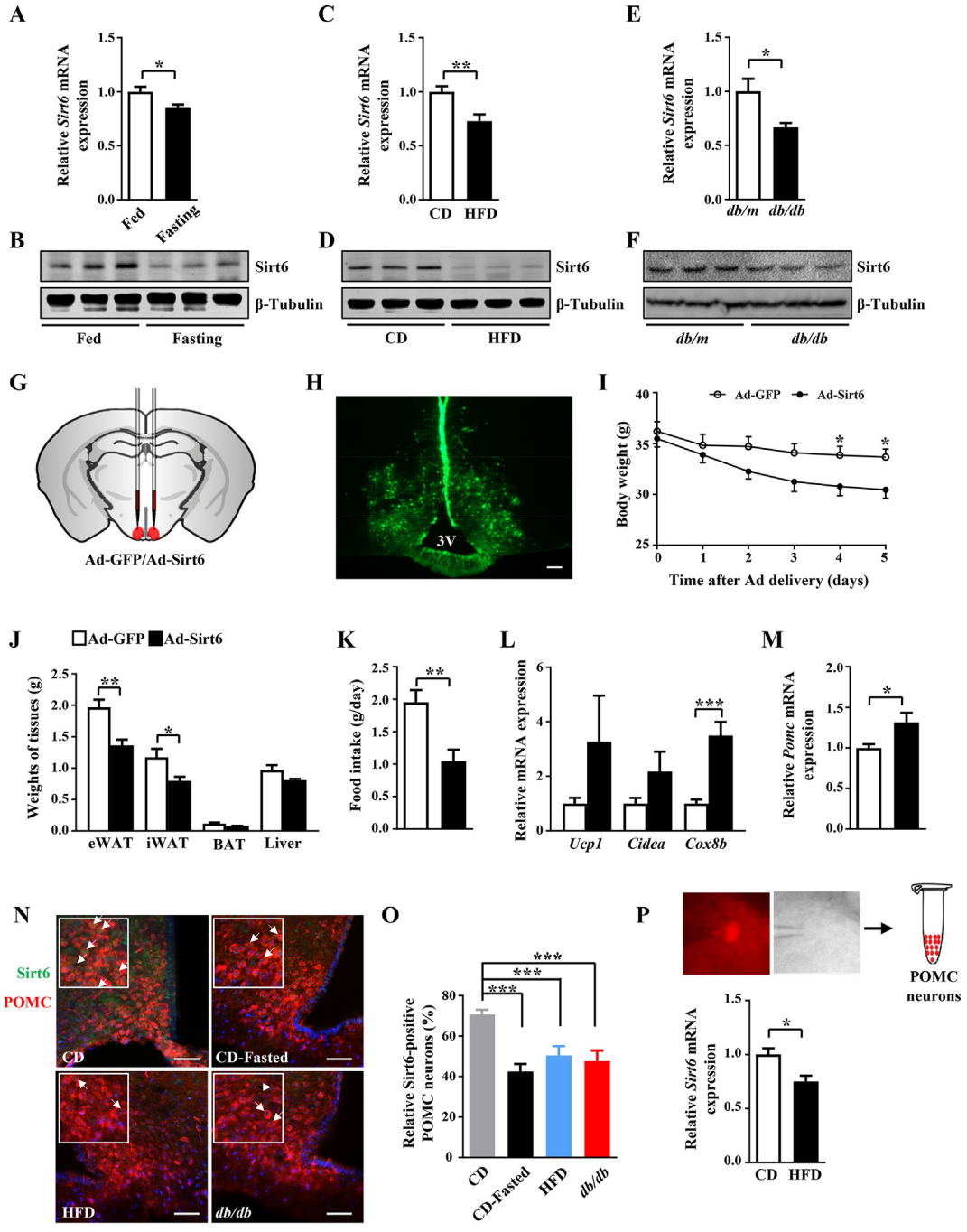

Figure 1: Overexpression of Sirt6 in the ARC ameliorates HFD-induced obesity. qPCR and western blot analysis of hypothalamic Sirt6 expression in fed (n = 9) or fasting (n = 8) mice (**A, B**), mice with a CD (n = 8) or an HFD (n = 8) (**C, D**), and *db/m* (n = 7) or *db/db* (n = 7) mice (**E, F**). (**G**) Schematic diagram of Ad-GFP or Ad-Sirt6 bilaterally injected into the ARC. (**H**) Localization of Ad-GFP (green) in the mouse ARC. 3V, third ventricle. Scale bar, 50 μm. Body weight profile (**I**) and adipose tissues and liver weight (**J**) in mice 7 days after adenovirus injection. (**K**) Daily food intake after Ad-GFP or Ad-Sirt6 injection (n = 5). (**L**) qPCR analysis of mRNA levels of browning-related genes in iWAT from mice injected with Ad-GFP or Ad-Sirt6 (n = 6). (**M**) *Pomc* mRNA levels in hypothalamic extracts from mice injected with Ad-GFP or Ad-Sirt6 (n = 5). Representative images (**N**) and quantification (**O**) of immunofluorescence staining of Sirt6 (green) in ARC POMC neurons (red) from mice under a normal chow diet (n = 15), fasting for 24 h (n = 17), HFD (n = 13), or from *db/db* mice (n = 12). Scale bar, 50 μm. (**P**) *Pomc*-tdTomato cells in the ARC from mice with a CD (n = 5) or an HFD (n = 4) were captured by using glass pipettes and used for the qPCR analysis of *Sirt6*. Data are mean ± SEM. $^{*}P < 0.05$, $^{**}P < 0.01$, $^{***}P < 0.001$. See also Supplementary Figure 1.

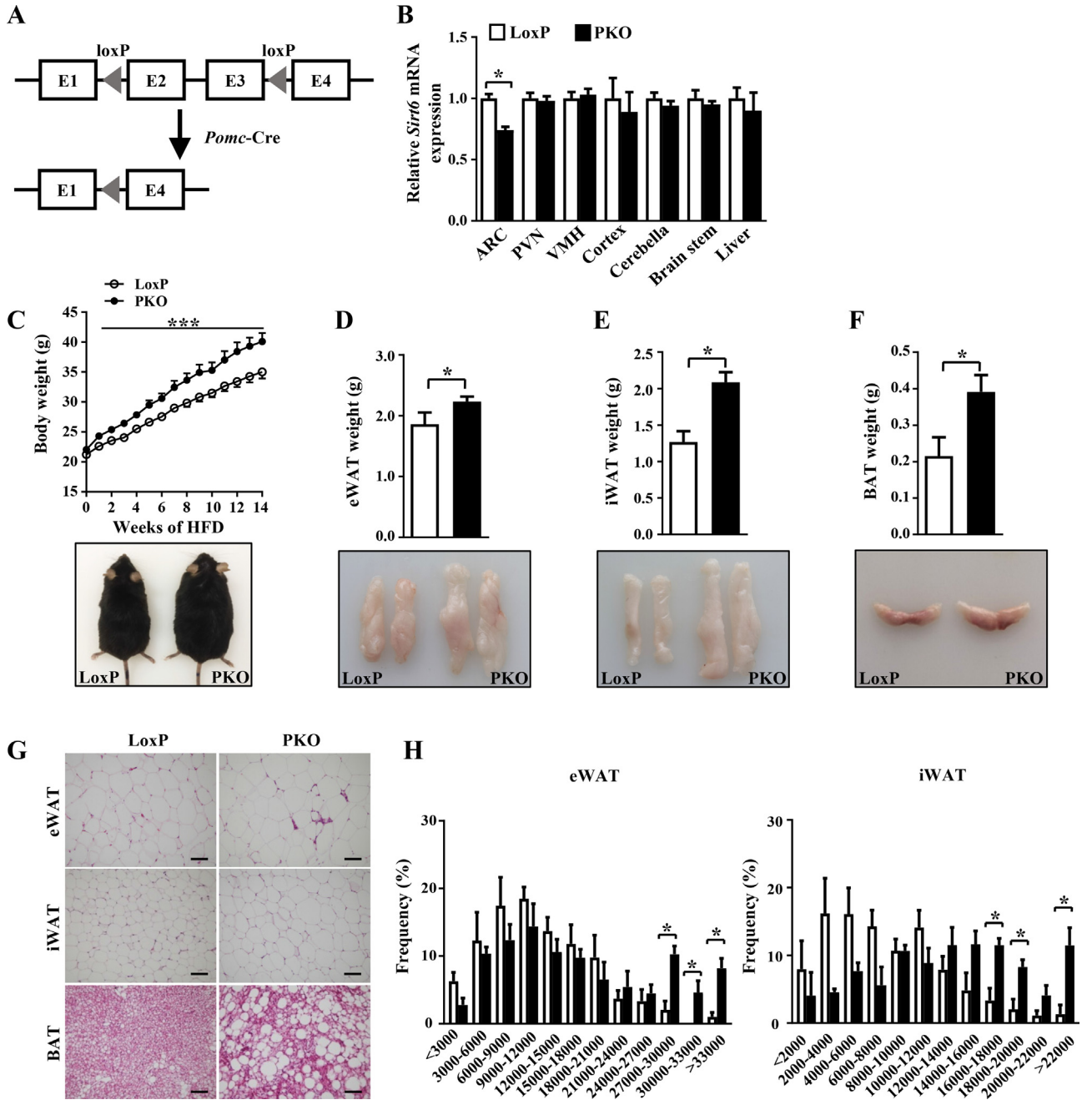

Figure 2: Selective deletion of Sirt6 in POMC-expressing cells predisposes mice to obesity under an HFD. (**A**) Schematic of genomic DNA region around exon 2 and exon 3 of *Sirt6* in mice. (**B**) *Sirt6* mRNA expression in different brain regions or tissues from LoxP (n = 8) and PKO (n = 9) mice. (**C**) The growth curve and a representative photograph for LoxP (n = 14) and PKO (n = 15) mice. Weight and representative photographs of eWAT (**D**), iWAT (**E**), and BAT (**F**) from 20-week-old LoxP (n = 8) and PKO (n = 15) mice. (**G**) Representative H&E-stained sections of eWAT, iWAT, and BAT from LoxP and PKO mice. Scale bar, 100 μm. (**H**) Frequency distribution of adipocyte cell size in eWAT and iWAT from LoxP and PKO mice fed with HFD. Data are mean ± SEM. $^{*}P < 0.05$, $^{***}P < 0.001$. See also Supplementary Figures 2–4.

(Supplementary Figure 3C). Therefore, both the hypoglycemia observed in the Sirt6 whole-body deficient mice and the growth retardation observed in the neuronal Sirt6-deficient mice were not due to the lack of Sirt6 in POMC neurons [19,21].

To assess whether energy balance is affected by POMC neuronal Sirt6 deficiency, we examined the body weight of LoxP and PKO mice fed with a CD or HFD. Under the CD, PKO mice showed a modest but significant increase in body weight as compared with control mice starting at age 11 weeks (Supplementary Figure 4A). Consistently, the adiposity was significantly increased, as evidenced by increased weight in eWAT, iWAT, and BAT (Supplementary Figure 4B–D). When challenged to HFD, PKO mice gained more weight than LoxP mice (Figure 2C). The higher body weight of PKO mice fed with HFD was also due to the increased weight of eWAT, iWAT, and BAT (Figure 2D–F). The higher weight of eWAT and iWAT in PKO mice likely resulted from the increased size of adipocytes under both the CD (Supplementary Figure 4E) and HFD (Figure 2G). The quantification of cell size further confirmed the H&E staining results (Figure 2H and

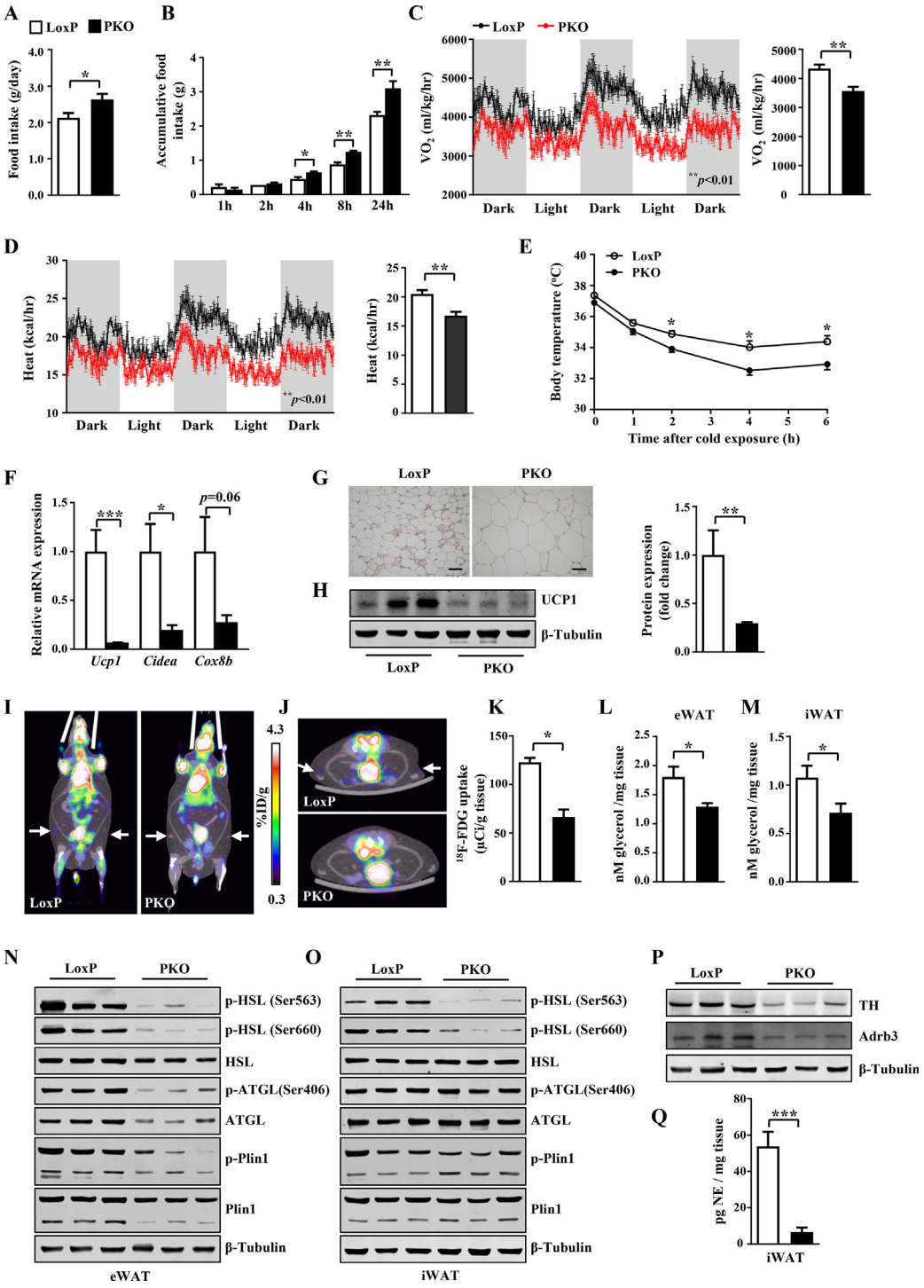

Figure 3: Sirt6 deficiency in POMC neurons causes increased food intake, reduced energy expenditure, and impaired browning and lipolytic functions of adipose tissues in mice fed with an HFD. (**A**) Food intake of LoxP (n = 7) and PKO (n = 4) mice under *ad libitum* feeding. (**B**) Accumulative food intake of LoxP (n = 5) and PKO (n = 4) mice after overnight fasting. O_2 consumption (**C**) and heat production (**D**) measured in LoxP and PKO mice (n = 4). (**E**) The rectal temperature of LoxP (n = 6) and PKO (n = 8) mice during acute cold exposure. (**F**) qPCR analysis of mRNA levels of browning-related genes in iWAT from LoxP and PKO mice (n = 8). Immunohistochemistry (**G**) and western blot analysis (**H**) of UCP1 protein levels in iWAT. Scale bar, 50 μm. (**I**–**K**) Representative ^{18}F-FDG PET-CT images and quantification of ^{18}F-FDG uptake in iWAT from LoxP (n = 6) and PKO (n = 5) mice. iWAT is indicated by white arrow. Basal lipolysis, as measured by glycerol release from eWAT (**L**) and iWAT (**M**) explants from 20-week-old LoxP and PKO mice (n = 6). Western blot analysis of protein levels of key lipolytic proteins in eWAT (**N**) and iWAT (**O**) from LoxP and PKO mice. (**P**) TH and Adrβ3 protein levels in iWAT determined by western blot analysis. (**Q**) NE content detected by high-performance liquid chromatography in iWAT from LoxP and PKO mice (n = 7). Data are mean ± SEM. $^{*}P < 0.05$, $^{**}P < 0.01$, $^{***}P < 0.001$. See also Supplementary Figure 5.

Supplementary Figure 4F). Collectively, these results demonstrate that Sirt6 in POMC neurons is a key component of the defense against obesity in mice under both a CD and an HFD.

3.4. PKO mice show impaired energy homeostasis

Energy homeostasis is maintained by a balance between energy intake and energy expenditure [1,2]. To identify the underlying mechanisms of the obesity observed in PKO mice, we assessed food intake, energy expenditure, and locomotor activity. Notably, an increase in food intake was observed under both conditions of *ad libitum* feeding (Figure 3A) or after overnight fasting in PKO mice (Figure 3B). The higher body weight in PKO mice was also associated with decreased energy expenditure, because O_2 consumption, heat production, and CO_2 production were significantly reduced (Figure 3C, D and Supplementary Figure 5A), with no change in physical activity (Supplementary Figure 5B). Consistently, when subjected to acute cold exposure, PKO mice showed a rapid decrease in rectal temperature under both the CD (Supplementary Figure 5C) and HFD (Figure 3E). The decreased energy expenditure and impaired adaptation to cold challenge in PKO mice could result from impaired thermogenesis of BAT or browning of iWAT. In BAT, no significant changes were observed in the mRNA and protein expression of UCP1 between LoxP and PKO mice (Supplementary Figure 5D–F), so the thermogenesis in BAT may not account for the decreased body temperature. In iWAT, the mRNA levels of *Ucp1* and *Cidea* were significantly suppressed in PKO mice (Figure 3F). Consistently, the protein expression of UCP1 was reduced in PKO mice as confirmed by immunohistochemistry and immunoblotting (Figure 3G, H). PET/CT with ^{18}F-FDG can image adaptive thermogenesis in iWAT [40]. As expected, PET/CT clearly showed a decrease in ^{18}F-FDG uptake in iWAT of PKO mice as compared with LoxP controls (Figure 3I–K). These results demonstrate that the obese phenotype observed in PKO mice was caused by hyperphagia and decreased energy expenditure.

Lipolysis is essential for thermogenesis because the fatty acids released from lipid mobilization serve as both obligatory activators for UCP1 and metabolic substrates fueling thermogenic respiration [41]. As expected, the rate of glycerol release was reduced in both eWAT and iWAT from PKO mice fed with an HFD (Figure 3L, M). Consistently, the key components in lipolytic pathways such as p-HSL, adipose triglyceride lipase (ATGL), and p-Plin1 were significantly suppressed (Figure 3N, O). Under a CD, PKO mice also exhibited a slight reduction in the lipolytic activity of eWAT and iWAT (Supplementary Figure 5G, H). The sympathetic nervous system (SNS) plays a key role in the lipolytic activity and browning of adipose tissue [42,43]. To determine whether the decreased browning and lipolysis in iWAT was associated with altered SNS function, we assessed the innervation of sympathetic neurons in iWAT and NE levels released from SNS. We found that the expression of tyrosine hydroxylase (TH), an enzyme required for the synthesis of catecholamines, as well as ADRB3, an NE receptor, was significantly reduced in iWAT from PKO mice (Figure 3P). Consistently, the NE level in iWAT was greatly reduced in PKO mice (Figure 3Q).

3.5. Sirt6 ablation in POMC neurons impairs leptin functions in the hypothalamus

To investigate the mechanisms underlying hyperphagia and decreased energy expenditure in PKO mice, we first assessed neuropeptide gene expression in the hypothalamus, including *Pomc*, *Cart*, *Agrp*, and *Npy*, which are known to play critical roles in regulating food intake and energy expenditure [2,8]. Under an HFD, the mRNA levels of *Cart*, *Agrp*, and *Npy* did not differ between genotypes, but the mRNA level of *Pomc* was downregulated significantly in PKO mice (Figure 4A). Consistently, the protein level of hypothalamic POMC was reduced, as detected by immunofluorescence and immunoblotting (Figure 4B, C and Supplementary Figure 6A). Consistently, the expression of α-MSH, a neuropeptide originated from POMC processing, was significantly decreased in the PVN of PKO mice (Supplementary Figure 6B). We did not observe significant changes in mRNA expressions of other hypothalamic hormones, including *Crh*, *Trh*, *Mch*, and *Orexin* (Supplementary Figure 6C).

Recent studies have revealed the pleiotropic actions of leptin, including the concurrent inhibition and activation of diverse hypothalamic neurons that lead to negative energy balance [44,45]. Thus, we postulated that the reduced POMC expression and the energy imbalance observed in PKO mice might be caused by impaired biologic actions of leptin. To test this possibility, we detected critical genes involved in the canonical leptin signaling pathway in the hypothalamus and found that the mRNA levels of *Jak2* and *Pi3k* were significantly downregulated in PKO mice (Figure 4D). The impaired leptin signaling was not due to a lower level of circulating leptin; instead, the serum level of leptin was higher in PKO mice under both a CD (Supplementary Figure 6D) and an HFD (Supplementary Figure 6E). To test whether the impaired leptin signaling was due to its resistance, we challenged mice with leptin and measured the leptin function and signaling pathway activity. To exclude the potential effect of food intake and body weight, we assessed leptin signaling in 6-week-old, CD-fed LoxP and PKO mice, which displayed similar body weight and adiposity between genotypes (data not shown). The effect of leptin on decreasing body weight and food intake was clearly detectable in 6-week-old LoxP mice but was significantly blunted in PKO mice (Figure 4E, F). Leptin drives lipolysis of peripheral WAT via sympathetic neuroadipose connections [46]. This effect was significantly blunted in PKO mice, as indicated by lower phosphorylation levels of key lipolytic proteins in both eWAT and iWAT (Figure 4G, H). In addition, leptin signaling pathway activity, as indicated by the level of phosphorylation of signal transducer and activator of transcription 3 (p-STAT3, Tyr705), was significantly reduced in PKO mice (Figure 4I, J and Supplementary Figure 6F). Collectively, these data suggest that Sirt6 in POMC neurons is necessary for maintaining the normal function of leptin.

3.6. Inhibition of Sirt6 diminishes leptin-induced depolarization of POMC cells

To further understand the mechanism of impaired function of leptin in PKO mice, we genetically marked POMC neurons by using Cre-dependent tdTomato-reporter mice (Figure 5A) and investigated the effect of leptin on the activity of POMC neurons in slice preparations. Electrophysiological recordings showed that the inhibition of Sirt6 by OSS_128,167, a known Sirt6 inhibitor [36,37], did not significantly affect the resting membrane potential of POMC neurons (Figure 5B–D). Upon leptin stimulation, POMC neurons quickly depolarized, as indicated by increased membrane potential. However, such depolarization was greatly blunted by Sirt6 inhibition (Figure 5E–G). These results further support that Sirt6 is required for normal responsiveness to leptin in POMC neurons.

3.7. Deletion of Sirt6 in POMC neurons impairs glucose homeostasis and promotes hepatic steatosis

Under a CD, PKO mice exhibited a slight impairment in GTT and ITT (Supplementary Figure 7A, B). When exposed to HFD, PKO mice displayed worse performance in both GTT and ITT (Figure 6A, B). In addition, no significant difference was observed in the serum levels of insulin and adiponectin between LoxP and PKO mice when fed with a CD (Supplementary Figure 7C, D). However, when exposed to

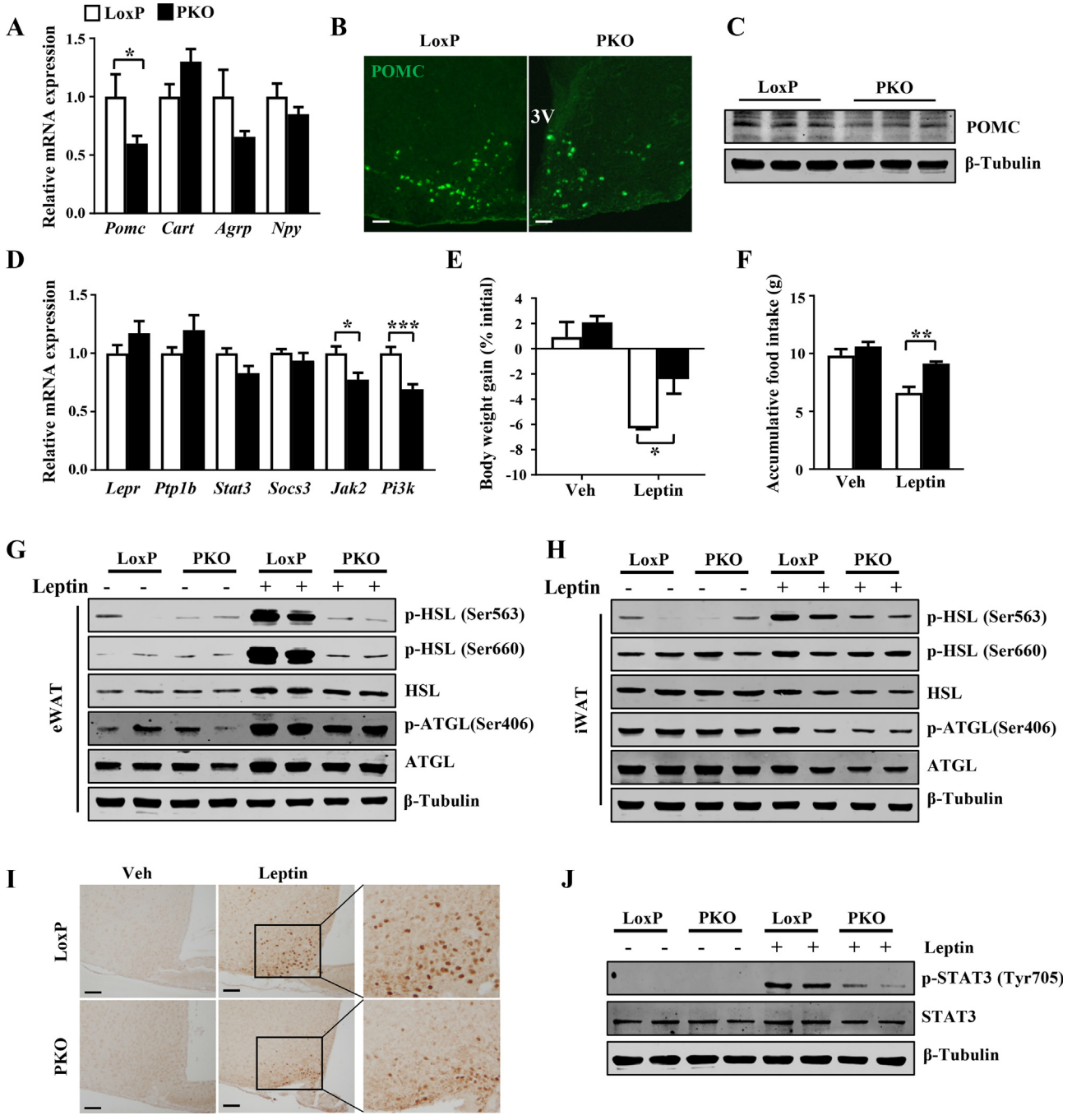

Figure 4: Sirt6 deletion in POMC neurons impairs hypothalamic POMC expression and leptin function. (**A**) qPCR analysis of hypothalamic neuropeptide expression in LoxP (n = 6) and PKO (n = 9) mice fed with an HFD. Immunofluorescence staining (**B**) and western blot analysis (**C**) of POMC in ARC of LoxP and PKO mice fed with an HFD. 3V, third ventricle. Scale bar, 50 μm. (**D**) qPCR analysis of genes related to leptin signaling pathways in hypothalamus from LoxP (n = 6) and PKO (n = 9) mice fed with an HFD. Body weight change (**E**) and accumulative food intake (**F**) in mice (6 weeks old) intraperitoneally injected with leptin (1 μg/g) for 3 days (n = 3). Western blot analysis of lipolytic enzymes in eWAT (**G**) and iWAT (**H**) of 6-week-old LoxP and PKO mice that received 500 ng/h recombinant leptin for 2 days. Representative immunohistochemical images (**I**) and western blot analysis (**J**) of p-STAT3 (Tyr705) in hypothalamus from 6-week-old LoxP and PKO mice 45 min after a single intraperitoneal injection of vehicle or leptin (1 μg/g). Scale bar, 100 μm. Data are mean ± SEM. $^{*}P < 0.05$, $^{**}P < 0.01$. See also Supplementary Figure 6.

HFD, significantly increased insulin level was observed in PKO mice (Figure 6C), despite serum adiponectin levels were unaffected (Figure 6D). When insulin signaling was assessed, insulin-stimulated phosphorylation of AKT (p-AKT) (Ser473) was attenuated in skeletal muscle in PKO mice fed with a CD (Supplementary Fig. 7E–H) and was further attenuated in the liver and skeletal muscle in PKO mice fed with an HFD (Figure 6E and Supplementary Figure 8A–C).

Hepatic steatosis is associated with obesity and insulin resistance. Under an HFD, PKO mice exhibited significantly increased lipid accumulation in the liver, as demonstrated by gross morphology, histological examination (H&E staining and Oil-red O staining), and elevated

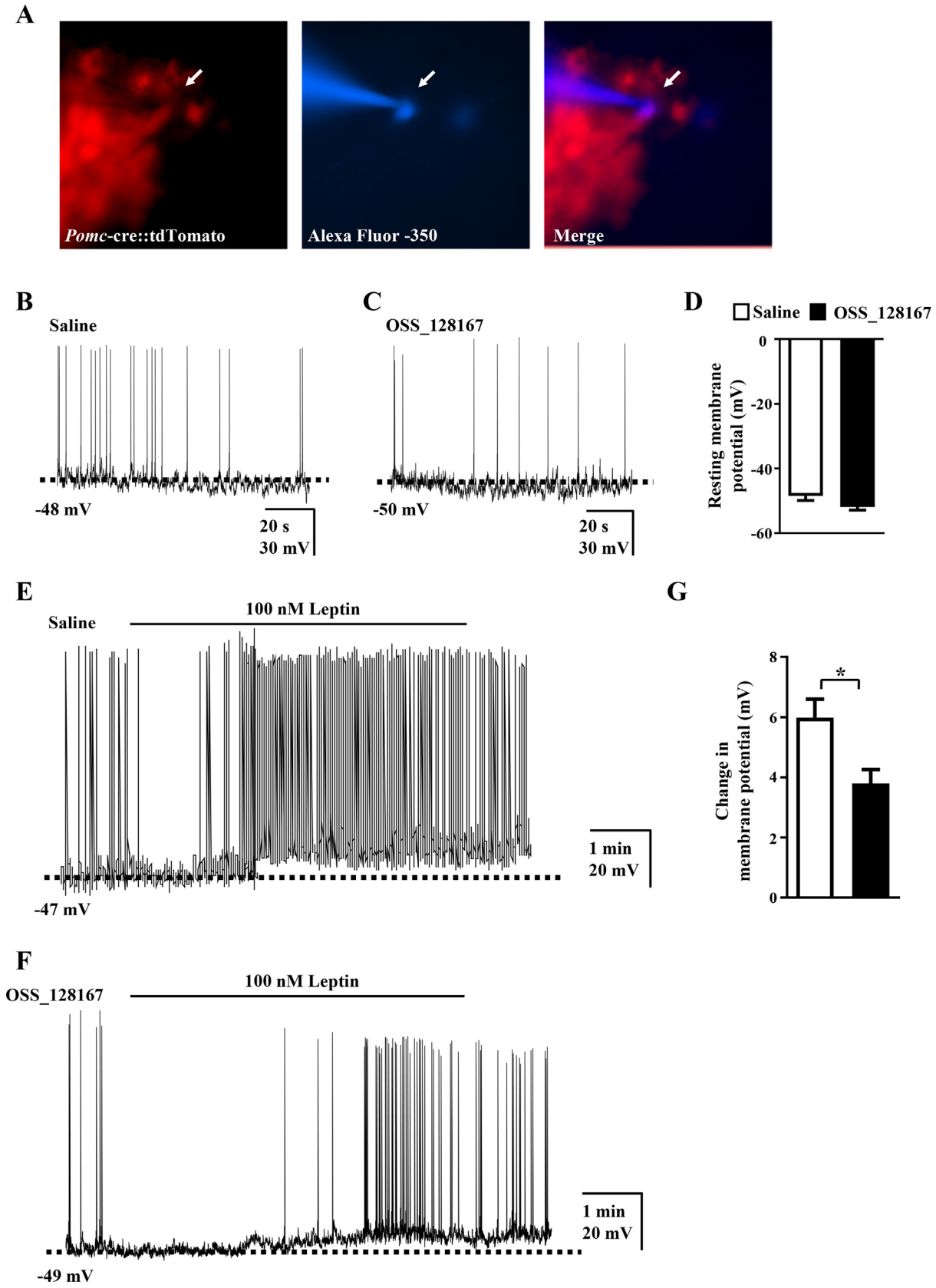

Figure 5: The inhibition of Sirt6 blunts the leptin-induced activation of POMC neurons. (**A**) POMC neurons from *Pomc*-Cre:tdTomato mice under TRITC (tdTomato) illumination, complete dialysis of Alexa Fluor-350 from the intracellular pipette, and merged image illustrate colocalization of tdTomato and Alexa Fluor 350 indicative of a POMC neuron. (**B**–**D**) Electrophysiological recording of POMC neurons with or without OSS_128,167 (100 μM) treatment (n = 10). (**E**–**G**) Electrophysiological recording of leptin-induced depolarization of POMC neurons with or without OSS_128,167 (100 μM) (n = 7). Data are mean ± SEM. $^{*}P < 0.05$.

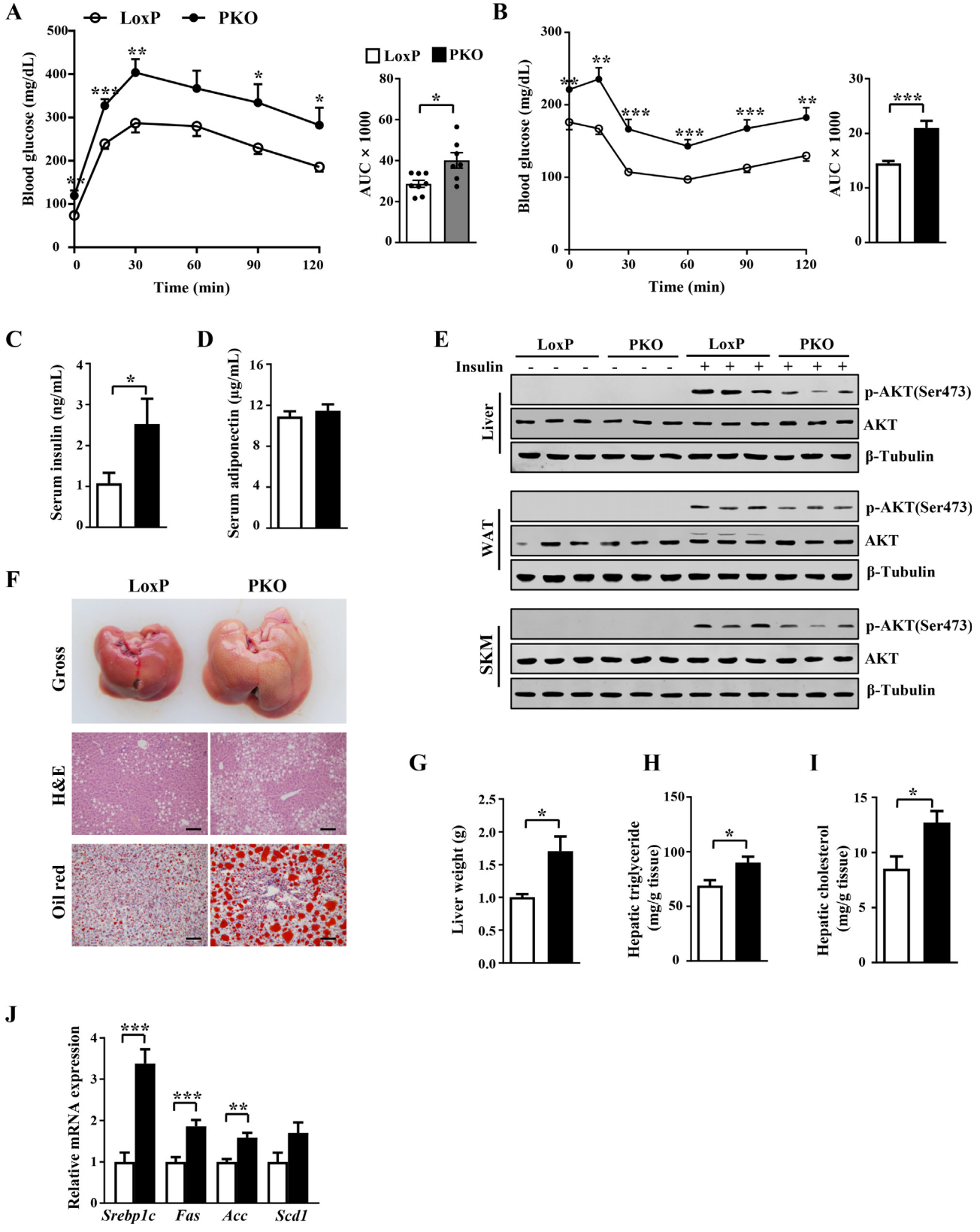

Figure 6: PKO mice exhibit impaired glucose homeostasis and promoted hepatic steatosis when fed with an HFD. (**A**) GTT in LoxP (n = 8) and PKO (n = 7) mice at age 20 weeks. (**B**) ITT in LoxP (n = 12) and PKO (n = 11) mice. (**C**) Serum insulin levels in overnight-fasting LoxP (n = 8) and PKO (n = 6) mice fed with an HFD. (**D**) Serum adiponectin levels in overnight-fasting LoxP and PKO mice fed with an HFD (n = 8). (**E**) Western blot analysis of AKT and p-AKT (Ser473) in the liver, adipose tissue, and skeletal muscle 15 min after the administration of insulin (1 U/kg). (**F**) Representative photographs, images of H&E- and Oil-red O-stained sections of LoxP and PKO mice at age 20 weeks. Scale bar, 100 μm. (**G**) Liver weight of LoxP (n = 8) and PKO (n = 16) mice at age 20 weeks. Hepatic TG (**H**) and TC (**I**) levels of LoxP (n = 11) and PKO (n = 18) mice at age 20 weeks. (**J**) qPCR determination of mRNA levels of hepatic lipogenesis genes from LoxP (n = 7) and PKO (n = 9) mice. Data are mean ± SEM. $^{*}P < 0.05$, $^{**}P < 0.01$, $^{***}P < 0.001$. See also Supplementary Figure 7–9.

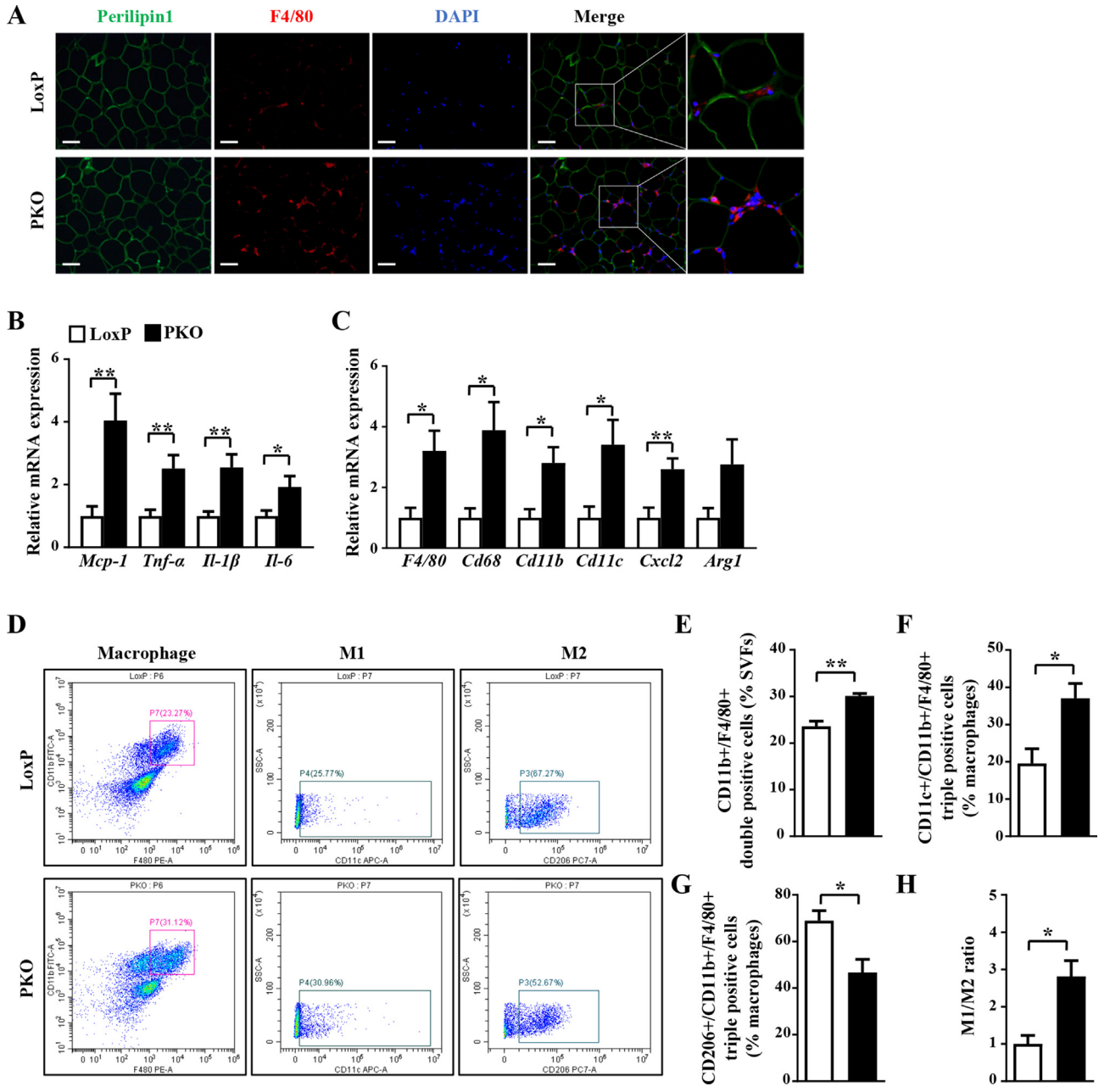

Figure 7: Ablation of Sirt6 in POMC neurons promotes adipose inflammation in mice fed with an HFD. (**A**) Immunofluorescence staining of F4/80 (red) and perilipin1 (green, a general marker of adipocytes) in eWAT from 20-week-old LoxP and PKO mice. Scale bar, 100 μm. (**B, C**) qPCR analysis of mRNA levels of macrophage markers and immune cell markers in eWAT from 20-week-old LoxP (n = 7) and PKO (n = 8) mice. (**D**–**H**) Flow cytometry of macrophages in eWAT from LoxP and PKO mice (n = 3). Data are mean ± SEM. $^{*}P < 0.05$, $^{**}P < 0.01$.

liver weight (Figure 6F, G). Moreover, hepatic lipid quantification showed higher levels of TG and TC in PKO mice (Figure 6H, I), with no changes in the liver of PKO mice under a CD (Supplementary Figure 9A–D). Lipogenic genes such as *Srebp1c*, *Fas*, and *Acc* were upregulated in the liver of PKO mice (Figure 6J).

3.8. Mice lacking Sirt6 in POMC neurons increase adipose tissue inflammation

Obesity may be associated with increased inflammation in adipose tissue [47]. When fed with an HFD, PKO mice showed a significant increase in F4/80-positive cells, as indicated by Perilipin1 (a general marker of adipocytes) and F4/80 double immunofluorescence staining (Figure 7A). Consistently, the gene expressions of inflammatory factors, including *Mcp-1*, *Tnf-α*, *Il-1β*, and *Il-6*, were all upregulated in PKO mice (Figure 7B). In addition, macrophage markers, including *F4/80*, *Cd68*, *Cd11b*, *Cd11c*, and *Cxcl2*, were markedly induced in eWAT from PKO mice (Figure 7C). However, no significant difference was observed in anti-inflammatory cytokine *Arg1* mRNA expression between LoxP and PKO mice (Figure 7C). Flow cytometry further confirmed that $CD11b^{+}/F4/80^{+}$ double-positive cells, which were macrophages, were induced in PKO mice (Figure 7D,E). Furthermore, as compared with controls, PKO mice showed a higher proportion of

M1-like macrophages ($CD11c^+CD11b^+F4/80^+$ triple-positive cells) (Figure 7D,F), a lower proportion of M2-like macrophages ($CD206^+CD11b^+$ $F4/80^+$ triple-positive cells) (Figure 7D,G), and a higher ratio of M1/M2 macrophages (Figure 7D,H).

4. DISCUSSION

Here, we show that Sirt6 in POMC neurons is an essential regulator of the whole-body energy homeostasis. The expression of Sirt6 in the hypothalamus and POMC neurons was reduced in fasting and obese mice. Hypothalamic ARC overexpression of Sirt6 ameliorated HFD-induced obesity. POMC neuron-specific deletion of Sirt6 caused obesity under both a CD and an HFD. The mechanistic study showed that Sirt6 ablation in POMC neurons significantly increased food intake and decreased energy expenditure. These observations may result from impaired leptin functions and sensitivity in POMC neurons when Sirt6 is absent. Moreover, PKO mice exhibited glucose intolerance and the fatty liver formation and greater inflammation in adipose tissues.

As an NAD^+-dependent deacetylase, Sirt6 has been reported to play key roles in aging, inflammation, and other pathological processes [12,48]. Particularly, Sirt6 expression is regulated by nutrient availability and plays critical roles in energy metabolism [13,49]. In the present study, we found that the expression of Sirt6 in the hypothalamus and POMC neurons was significantly decreased upon fasting. However, a previous study reported its increased expression in the whole brain of mice after 24-hour fasting [49]. This discrepancy might indicate that Sirt6 expression might be differentially regulated in different brain areas by fasting. We also reported downregulated Sirt6 levels in the hypothalamus and POMC neurons of diet- and genetically induced obese models. The reduction of Sirt6 in both physiological and pathophysiological conditions suggests a critical role of Sirt6 in the hypothalamus and POMC neurons for the response to metabolic shift and diet challenges, providing a link between nutrient availability and energy balance.

Our results suggest that Sirt6 in POMC neurons directly controls the whole-body energy homeostasis. Sirt6 overexpression decreased whereas Sirt6 deletion in POMC neurons exacerbated the body weight gain. Sirt6-regulated obesity might be due to its modulation of food intake and energy expenditure in POMC neurons, known as an essential molecular component in energy homeostasis [50]. The POMC neurons sense peripheral signals, including multiple hormones and nutrients such as leptin, an adipocyte-derived hormone, which plays a prominent role in the regulation of POMC neurons [44]. In POMC neurons, leptin enhances the transcription of the *Pomc* gene and induces POMC neuronal depolarization through JAK-STAT3 signaling, which serves as a marker of leptin signaling activity [44]. The impaired signaling or defects in the downstream neural circuitry that responds to leptin might cause leptin resistance, a major barrier to combating obesity. In the present study, Sirt6 was a critical molecular component of leptin-sensing mechanisms in POMC neurons. Indeed, our results demonstrate that Sirt6 deletion in POMC neurons impaired leptin sensitivity, as the leptin-induced activation of the JAK-STAT3 signaling cascade was impaired, and its effect on decreasing body weight and food intake was blunted. Electrophysiological studies further confirmed that leptin-induced POMC neuronal membrane potential was severely compromised with Sirt6 inhibition. These results strongly argue that the effect of POMC neuronal Sirt6 deficiency to blunt leptin signaling underlies the effect of POMC neuronal function, which, further, promotes the whole-body energy imbalance. Future studies are needed to fully reveal the intracellular targets of Sirt6 in modulating leptin signaling pathways.

As a group of anorexia cells, POMC neurons tightly control feeding behavior [2,50]. Upon nutrient ingestion, POMC is cleaved to the anorexigenic neuropeptide α-melanocyte-stimulating hormone (α-MSH) by posttranscriptional processing. By binding to the MC3R or MC4R on downstream neurons, α-MSH activates catabolic pathways and suppresses food intake [51]. Both reduced POMC neuronal activity or impaired posttranscriptional processing can lead to hyperphagia. The increase in food intake after Sirt6 deletion in POMC neurons we found may result from reduced POMC expression level and/or neuronal activity, because genes related to posttranscriptional processing were not affected (data not shown).

Adipose tissues are tightly innervated by the SNS, which results from complex central networks including POMC neurons [45]. By receiving and integrating several peripheral signals, ARC POMC neurons send projections to various nuclei including the PVN, DMH, VMH, and other brain regions [11,52]. MC4R-expressing neurons in these regions are polysynaptically connected to adipose tissue and play critical roles in regulating the SNS outflow to these adipose depots [45]. Thus, POMC neurons are important for mediating sympathetic nervous activity-dependent adipocyte metabolism. Indeed, we found that POMC neuronal Sirt6 deficiency decreased the sympathetic nerve innervation (as shown by decreased expression of TH) and sympathetic nerve activity (lower level of NE) in iWAT.

Activation of the SNS in WAT stimulates adipocyte lipolysis [34]. The NE released from SNS binds to β3-ARs on adipocytes and activates PKA, which phosphorylates HSL and perilipin-1 to break down triglycerides and generate fatty acids and glycerol [42,43]. In the present study, the lipolytic activity of both eWAT and iWAT was significantly reduced in PKO mice. To further prove that this reduced lipolytic activity was resulted from lower sympathetic nerve activity, we injected mice with leptin, which is known to increase the sympathetic efferent signal to WAT to induce lipolysis [34]. Leptin could stimulate lipolysis in LoxP but not PKO mice, so the POMC-derived SNS activity was indeed compromised in PKO mice.

In conclusion, our results identify Sirt6 as an essential molecular regulator for POMC neurons to regulate energy homeostasis. The overexpression of Sirt6 significantly ameliorated HFD-induced obesity in mice. Conversely, Sirt6 deficiency in POMC neurons promoted body weight gain under both a CD and an HFD because of the induced food intake and reduced energy expenditure. The mechanistic study indicated that Sirt6 deficiency compromised leptin activity in POMC neurons. These results further support that Sirt6 is an important molecular regulator to maintain the whole-body energy homeostasis.

AUTHORS' CONTRIBUTIONS

Q. T., Y. G., Y. C. and J. H. designed the experiments; Q. T. and Y. G. performed experiments. Q. L., X. Y., T. W., C. H., Y. H., J. Z., Z. Z., R. L., S. P., G. Z., Y. Z., J. Z., H. H., and Y. L. helped with experiments. W. J. contributed to the discussion and reviewed the manuscript. Q. T. and J. H. wrote the manuscript. J. H. obtained funding. T. W. and J. H. are the guarantors of this work and, as such, had full access to all the data in the study and take responsibility for the integrity of the data and the accuracy of the data analysis.

ACKNOWLEDGMENTS

This work was supported by the National Natural Science Foundation of China (81930020, 81873662, and 81870599), research funding from Sichuan Province (2018SZ0158), China Postdoctoral Fellowship (2017M612981), Young Scientist Fellowship of Sichuan University (2017SCU11026), and Postdoctoral Fellowship of Sichuan University (2017SCU12036). The authors thank Miss Li Li and Miss Fei Chen from the Laboratory of Pathology, West China Hospital, for technical assistance.

CONFLICT OF INTEREST

The authors declare no competing financial interests.

APPENDIX A. SUPPLEMENTARY DATA

Supplementary data to this article can be found online at https://doi.org/10.1016/j.molmet.2020.100994.

REFERENCES

[1] Nadal, A., Quesada, I., Tuduri, E., Nogueiras, R., Alonso-Magdalena, P., 2017. Endocrine-disrupting chemicals and the regulation of energy balance. Nature Reviews Endocrinology 13(9):536–546.

[2] van der Klaauw, A.A., Farooqi, I.S., 2015. The hunger genes: pathways to obesity. Cell 161(1):119–132.

[3] Upadhyay, J., Farr, O., Perakakis, N., Ghaly, W., Mantzoros, C., 2018. Obesity as a disease. Medical Clinics of North America 102(1):13–33.

[4] Roh, E., Song, D.K., Kim, M.S., 2016. Emerging role of the brain in the homeostatic regulation of energy and glucose metabolism. Experimental & Molecular Medicine 48:e216.

[5] Myers Jr., M.G., Olson, D.P., 2012. Central nervous system control of metabolism. Nature 491(7424):357–363.

[6] Carmo-Silva, S., Cavadas, C., 2017. Hypothalamic dysfunction in obesity and metabolic disorders. Advances in Cellular Neurobiology 19:73–116.

[7] Shen, W.J., Yao, T., Kong, X., Williams, K.W., Liu, T., 2017. Melanocortin neurons: multiple routes to regulation of metabolism. Biochimica et Biophysica Acta - Molecular Basis of Disease 1863(10 Pt A):2477–2485.

[8] Balthasar, N., Dalgaard, L.T., Lee, C.E., Yu, J., Funahashi, H., Williams, T., et al., 2005. Divergence of melanocortin pathways in the control of food intake and energy expenditure. Cell 123(3):493–505.

[9] Yaswen, L., Diehl, N., Brennan, M.B., Hochgeschwender, U., 1999. Obesity in the mouse model of pro-opiomelanocortin deficiency responds to peripheral melanocortin. Nature Medicine 5(9):1066–1070.

[10] Krude, H., Biebermann, H., Luck, W., Horn, R., Brabant, G., Gruters, A., 1998. Severe early-onset obesity, adrenal insufficiency and red hair pigmentation caused by POMC mutations in humans. Nature Genetics 19(2):155–157.

[11] Waterson, M.J., Horvath, T.L., 2015. Neuronal regulation of energy homeostasis: beyond the hypothalamus and feeding. Cell Metabolism 22(6):962–970.

[12] Kuang, J., Chen, L., Tang, Q., Zhang, J., Li, Y., He, J., 2018. The role of Sirt6 in obesity and diabetes. Frontiers in Physiology 9:135.

[13] Kim, H.S., Xiao, C., Wang, R.H., Lahusen, T., Xu, X., Vassilopoulos, A., et al., 2010. Hepatic-specific disruption of SIRT6 in mice results in fatty liver formation due to enhanced glycolysis and triglyceride synthesis. Cell Metabolism 12(3):224–236.

[14] Xiong, X., Wang, G., Tao, R., Wu, P., Kono, T., Li, K., et al., 2016. Sirtuin 6 regulates glucose-stimulated insulin secretion in mouse pancreatic beta cells. Diabetologia 59(1):151–160.

[15] Cui, X., Yao, L., Yang, X., Gao, Y., Fang, F., Zhang, J., et al., 2017. SIRT6 regulates metabolic homeostasis in skeletal muscle through activation of AMPK. American Journal of Physiology Endocrinology and Metabolism 313(4):E493–E505.

[16] Kuang, J., Zhang, Y., Liu, Q., Shen, J., Pu, S., Cheng, S., et al., 2017. Fat-specific Sirt6 ablation sensitizes mice to high-fat diet-induced obesity and insulin resistance by inhibiting lipolysis. Diabetes 66(5):1159–1171.

[17] Yao, L., Cui, X., Chen, Q., Yang, X., Fang, F., Zhang, J., et al., 2017. Cold-inducible SIRT6 regulates thermogenesis of Brown and beige fat. Cell Reports 20(3):641–654.

[18] Chen, L., Liu, Q., Tang, Q., Kuang, J., Li, H., Pu, S., et al., 2019. Hepatocyte-specific Sirt6 deficiency impairs ketogenesis. Journal of Biological Chemistry 294(5):1579–1589.

[19] Mostoslavsky, R., Chua, K.F., Lombard, D.B., Pang, W.W., Fischer, M.R., Gellon, L., et al., 2006. Genomic instability and aging-like phenotype in the absence of mammalian SIRT6. Cell 124(2):315–329.

[20] Liszt, G., Ford, E., Kurtev, M., Guarente, L., 2005. Mouse Sir2 homolog SIRT6 is a nuclear ADP-ribosyltransferase. Journal of Biological Chemistry 280(22):21313–21320.

[21] Schwer, B., Schumacher, B., Lombard, D.B., Xiao, C., Kurtev, M.V., Gao, J., et al., 2010. Neural sirtuin 6 (Sirt6) ablation attenuates somatic growth and causes obesity. Proceedings of the National Academy of Sciences of the United States of America 107(50):21790–21794.

[22] He, Jinhan, Gao, J., Xu, Meishu, Ren, Songrong, Stefanovic-Racic, Maja, O'Doherty, Robert Martin, et al., 2013. PXR ablation alleviates diet-induced and genetic obesity and insulin resistance in mice. Diabetes.

[23] Cheng, S., Zou, M., Liu, Q., Kuang, J., Shen, J., Pu, S., et al., 2017. Activation of constitutive androstane receptor prevents cholesterol gallstone formation. American Journal of Pathology 187(4):808–818.

[24] Mo, L., Shen, J., Liu, Q., Zhang, Y., Kuang, J., Pu, S., et al., 2016. Irisin is regulated by CAR in liver and is a mediator of hepatic glucose and lipid metabolism. Molecular Endocrinology 30(5):533–542.

[25] Jaworski, K., Ahmadian, M., Duncan, R.E., Sarkadi-Nagy, E., Varady, K.A., Hellerstein, M.K., et al., 2009. AdPLA ablation increases lipolysis and prevents obesity induced by high-fat feeding or leptin deficiency. Nature Medicine 15(2):159–168.

[26] Zu, L., He, J., Jiang, H., Xu, C., Pu, S., Xu, G., 2009. Bacterial endotoxin stimulates adipose lipolysis via toll-like receptor 4 and extracellular signal-regulated kinase pathway. Journal of Biological Chemistry 284(9):5915–5926.

[27] Liew, C.W., Boucher, J., Cheong, J.K., Vernochet, C., Koh, H.-J., Mallol, C., et al., 2013. Ablation of TRIP-Br2, a regulator of fat lipolysis, thermogenesis and oxidative metabolism, prevents diet-induced obesity and insulin resistance. Nature Medicine 19(2):217–226.

[28] Herzer, S., Meldner, S., Grone, H.J., Nordstrom, V., 2015. Fasting-induced lipolysis and hypothalamic insulin signaling are regulated by neuronal glucosylceramide synthase. Diabetes 64(10):3363–3376.

[29] Xiao, Y., Deng, Y., Yuan, F., Xia, T., Liu, H., Li, Z., et al., 2017. ATF4/ATG5 signaling in hypothalamic proopiomelanocortin neurons regulates fat mass via affecting energy expenditure. Diabetes 66(5):1146–1158.

[30] Stump, M., Guo, D.F., Lu, K.T., Mukohda, M., Liu, X., Rahmouni, K., et al., 2016. Effect of selective expression of dominant-negative PPARgamma in pro-opiomelanocortin neurons on the control of energy balance. Physiological Genomics 48(7):491–501.

[31] Chen, Y., Wu, R., Chen, H.Z., Xiao, Q., Wang, W.J., He, J.P., et al., 2015. Enhancement of hypothalamic STAT3 acetylation by nuclear receptor Nur77 dictates leptin sensitivity. Diabetes 64(6):2069–2081.

[32] Dodd, G.T., Decherf, S., Loh, K., Simonds, S.E., Wiede, F., Balland, E., et al., 2015. Leptin and insulin act on POMC neurons to promote the browning of white fat. Cell 160(1–2):88–104.

[33] Ren, H., Cook, J.R., Kon, N., Accili, D., 2015. Gpr17 in AgRP neurons regulates feeding and sensitivity to insulin and leptin. Diabetes 64(11):3670–3679.

[34] Zeng, W., Pirzgalska, R.M., Pereira, M.M., Kubasova, N., Barateiro, A., Seixas, E., et al., 2015. Sympathetic neuro-adipose connections mediate leptin-driven lipolysis. Cell 163(1):84–94.

[35] Yao, T., Deng, Z., Gao, Y., Sun, J., Kong, X., Huang, Y., et al., 2017. Ire1α in Pomc neurons is required for thermogenesis and glycemia. Diabetes 66(3):663–673.

[36] Parenti, M.D., Grozio, A., Bauer, I., Galeno, L., Damonte, P., Millo, E., et al., 2014. Discovery of novel and selective SIRT6 inhibitors. Journal of Medicinal Chemistry 57(11):4796–4804.

[37] Cea, M., Cagnetta, A., Adamia, S., Acharya, C., Tai, Y.T., Fulciniti, M., et al., 2016. Evidence for a role of the histone deacetylase SIRT6 in DNA damage response of multiple myeloma cells. Blood 127(9):1138—1150.

[38] Pu, S., Ren, L., Liu, Q., Kuang, J., Shen, J., Cheng, S., et al., 2016. Loss of 5-lipoxygenase activity protects mice against paracetamol-induced liver toxicity. British Journal of Pharmacology 173(1):66—76.

[39] Kaluski, S., Portillo, M., Besnard, A., Stein, D., Einav, M., Zhong, L., et al., 2017. Neuroprotective functions for the histone deacetylase SIRT6. Cell Reports 18(13):3052—3062.

[40] Park, J.W., Jung, K.H., Lee, J.H., Quach, C.H., Moon, S.H., Cho, Y.S., et al., 2015. 18F-FDG PET/CT monitoring of beta3 agonist-stimulated brown adipocyte recruitment in white adipose tissue. Journal of Nuclear Medicine 56(1):153—158.

[41] Divakaruni, A.S., Humphrey, D.M., Brand, M.D., 2012. Fatty acids change the conformation of uncoupling protein 1 (UCP1). Journal of Biological Chemistry 287(44):36845—36853.

[42] Fedorenko, A., Lishko, P.V., Kirichok, Y., 2012. Mechanism of fatty-acid-dependent UCP1 uncoupling in brown fat mitochondria. Cell 151(2):400—413.

[43] Kazak, L., Chouchani, E.T., Jedrychowski, M.P., Erickson, B.K., Shinoda, K., Cohen, P., et al., 2015. A creatine-driven substrate cycle enhances energy expenditure and thermogenesis in beige fat. Cell 163(3):643—655.

[44] Kwon, O., Kim, K.W., Kim, M.S., 2016. Leptin signalling pathways in hypothalamic neurons. Cellular and Molecular Life Sciences 73(7):1457—1477.

[45] Richard, D., 2015. Cognitive and autonomic determinants of energy homeostasis in obesity. Nature Reviews Endocrinology 11(8):489—501.

[46] Jiang, H., Ding, X., Cao, Y., Wang, H., Zeng, W., 2017. Dense intra-adipose sympathetic arborizations are essential for cold-induced beiging of mouse white adipose tissue. Cell Metabolism 26(4):686—692 e683.

[47] Olefsky, J.M., Glass, C.K., 2010. Macrophages, inflammation, and insulin resistance. Annual Review of Physiology 72:219—246.

[48] Bae, E.J., 2017. Sirtuin 6, a possible therapeutic target for type 2 diabetes. Archives of Pharmacal Research 40(12):1380—1389.

[49] Kanfi, Y., Shalman, R., Peshti, V., Pilosof, S.N., Gozlan, Y.M., Pearson, K.J., et al., 2008. Regulation of SIRT6 protein levels by nutrient availability. FEBS Letters 582(5):543—548.

[50] Toda, C., Santoro, A., Kim, J.D., Diano, S., 2017. POMC neurons: from birth to death. Annual Review of Physiology 79:209—236.

[51] Nillni, E.A., 2007. Regulation of prohormone convertases in hypothalamic neurons: implications for prothyrotropin-releasing hormone and proopiomelanocortin. Endocrinology 148(9):4191—4200.

[52] Kleinridders, A., Konner, A.C., Bruning, J.C., 2009. CNS-targets in control of energy and glucose homeostasis. Current Opinion in Pharmacology 9(6):794—804.

